Weierstraß-Institut
für Angewandte Analysis und Stochastik

im Forschungsverbund Berlin e.V.

Preprint ISSN 0946 – 8633

Stabilized finite element schemes for incompressible flow using Scott-Vogelius elements

E. Burman [1], A. Linke [2]

submitted: September 20, 2006

[1] Institute of Analysis and Scientific Computing
Ecole Polytechnique Federale de Lausanne
Lausanne, 1015
Switzerland
e-mail: erik.burman@epfl.ch

[2] Weierstrass Institute for Applied Analysis and Stochastics
Mohrenstr. 39
10117 Berlin
Germany
e-mail: linke@wias-berlin.de

No. 1165
Berlin 2006

2000 *Mathematics Subject Classification.* 65M12, 65M15, 76M10.

Key words and phrases. mixed finite elements, stabilized methods, solenoidal finite elements, edge stabilization, interior penalty, local projection, Oseen's equation, LBB-condition, a-priori estimate.

Edited by
Weierstraß-Institut für Angewandte Analysis und Stochastik (WIAS)
Mohrenstraße 39
10117 Berlin
Germany

Fax: + 49 30 2044975
E-Mail: preprint@wias-berlin.de
World Wide Web: http://www.wias-berlin.de/

Abstract

We propose a stabilized finite element method based on the Scott-Vogelius element in combination with either a local projection stabilization or an edge oriented stabilization based on a penalization of the gradient jumps over element edges. We prove a discrete inf-sup condition leading to optimal a priori error estimates. The theoretical considerations are illustrated by some numerical examples.

1 Introduction

The approximation of flow at high Reynolds numbers remains a challenging task. In fact due to the energy conservation properties of the standard Galerkin method and the fact that the incompressibility condition is satisfied only weakly the standard Galerkin finite element method fails when the local Reynolds number is high even in the linearized case. The reason for this is essentially the fact that the viscous dissipation is too small compared to the convection term or the term imposing incompressibility. When these non-symmetric terms are big the solution may be polluted by spurious oscillations. In order to counter these effects stabilized finite element methods have been proposed, taking its origin in the SUPG method. One can distinguish two cases:

(1) use of equal order interpolation for velocities and pressure
(2) use of an LBB-stable velocity-pressure pair.

In the first case the inf-sup condition on discrete level is satisfied thanks to some pressure stabilization technique. However, for both cases effects due to dominating convection *and* effects due to insufficient control of the incompressibility condition must be stabilized. For stabilized methods applied to the incompressible Navier-Stokes' equation or Oseen's problem we refer to the work of Johnson and Saranen [19], Hansbo and Szepessy [17], Tobiska and Verfürth [26], and Franca and Frey [12] in the case of SUPG type stabilizations and Braack and Burman [3] and Burman et al. [5] in the case of more recent advances using local projection or interior penalty stabilization with equal order interpolation. For work on inf-sup stable elements with stabilization we refer to Lube et al. [15] for SUPG type stabilization and Burman and Hansbo [8] or Burman and Fernàndez [6] for interior penalty type stabilizations.

In numerical experiments it has been observed that when using equal order interpolation the stabilization of the divergence only introduces additional damping and it is unclear if it is necessary in practice. The situation is different in the case of LBB-stable velocity-pressure pairs, here additional stabilization

of the divergence turns out to be of importance both from a theoretical and numerical point of view, see [15,21]. This is awkward since the term stabilizing the divergence is ill-conditioned, and may introduce additional couplings in the system matrix. In this paper we propose to use the lowest order Scott-Vogelius element [25,27] for the computation of incompressible flows. In two space dimensions this element corresponds to piecewise quadratic continuous interpolation for the velocities and piecewise affine discontinuous interpolation for the pressure. Satisfaction of the inf-sup condition is obtained thanks to a macro element structure of the computational mesh. It follows that the divergence of the velocity space is included in the pressure space and hence the discrete inf-sup condition gives control also of the divergence of the velocities in norm L^2. In fact, if we consider incompressible flow, the discrete solution will be pointwise divergence free. Thanks to this fact we do not need to consider any stabilization of the divergence. The only stabilization term added is a term needed to control spurious oscillations due to dominating convection. In the first part of the paper we consider an abstract form of the stabilization operator, specifying what conditions have to be satisfied for the error analysis to hold. We then give two examples of stabilization operators that satisfy the conditions: the local projection stabilization of Becker and Braack and the interior penalty stabilization proposed by Burman and Hansbo. It should be noted that one might just as well consider a turbulence model based on physical considerations. The error analysis below (valid for smooth solutions) will then be conditioned by the weak-consistency properties of the turbulence model.

An outline of the paper is as follows: in the Section 2 we introduce the Oseen's equation which will serve as linear model problem, in Section 3 we propose a finite element discretization of the model problem based on the Scott-Vogelius element and a stabilization operator for the convective terms. Then in Section 4 we prove an inf-sup condition giving control both of the L^2-norm of the pressure and the L^2-norm of the divergence of the velocities. Using the inf-sup condition we then prove an error estimate in a norm that is dominated by the H^1 norm of the velocities in the low Reynolds number regime and by the $H(\mathrm{div})$ norm of the velocities in the high Reynolds number regime. In Section 5 we show how two different stabilization operators enter the framework proposed in the previous section. Finally in Section 6 we give some numerical illustrations using the Scott-Vogelius element in combination with the interior penalty stabilization on gradient jumps.

2 Continuous Oseen equation

We consider the generalized Oseen equation for $(\mathbf{u}, p)$ in a polyhedral domain $\Omega \subset \mathbb{R}^d$, $d \in \{2, 3\}$,

$$\begin{aligned} -\nu\Delta\mathbf{u} + \mathbf{a}\cdot\nabla\mathbf{u} + \alpha\mathbf{u} + \nabla p &= \mathbf{f} && \text{in } \Omega \\ -\nabla\cdot\mathbf{u} &= g && \text{in } \Omega \\ \mathbf{u} &= 0 && \text{on } \partial\Omega, \end{aligned} \tag{1}$$

where $\mathbf{u}, \mathbf{a} \in [H_0^1(\Omega)]^d =: V^d$, $\mathbf{a} \in [W^{1,\infty}(\Omega)]^d \cap \mathbf{H}(\Omega)$, $p, g \in L_0^2(\Omega) =: Q$, $\mathbf{f} \in [L^2(\Omega)]^d$. By $\mathbf{H}(\Omega)$ we denote the functions $\mathbf{u} \in [L^2(\Omega)]^d$ such that $\nabla\cdot\mathbf{u} = 0$ and $\mathbf{u}\cdot\mathbf{n} = 0$ on $\partial\Omega$. $L_0^2(\Omega)$ is the subset of $L^2(\Omega)$ with zero average. ν and α are positive scalars, $\mathbf{f}$ and g are given source terms. Usually, the Oseen problem is a result of linearization of the Navier-Stokes problem. Then $\mathbf{a}$ is a finite element velocity field. In the following we will use the notation $a \lesssim b$ for $a \le Cb$, where the constant C is independent of the mesh size and the parameters ν and α, but not of the local mesh geometry.

The variational formulation of this problem is to find $(\mathbf{u}, p) \in X := V^d \times Q$ such that

$$A[(\mathbf{u}, p), (\mathbf{v}, q)] = (\mathbf{f}, \mathbf{v}) + (g, q), \tag{2}$$

for all $(\mathbf{v}, q) \in X$, where

$$\begin{aligned} A[(\mathbf{u}, p), (\mathbf{v}, q)] &:= a(\mathbf{u}, \mathbf{v}) + b(p, \mathbf{v}) + b(q, \mathbf{u}) \\ a(\mathbf{u}, \mathbf{v}) &:= \nu(\nabla\mathbf{u}, \nabla\mathbf{v}) + (\mathbf{a}\cdot\nabla\mathbf{u}, \mathbf{v}) + \alpha(\mathbf{u}, \mathbf{v}) \\ b(p, \mathbf{v}) &:= -(p, \nabla\cdot\mathbf{v})). \end{aligned} \tag{3}$$

Here, $(\cdot,\cdot)$ denotes the L_2-scalar product and $\|\cdot\|_{0,\Omega}$ is the corresponding norm. The standard Sobolev norm of the Hilbert space $[H^s(\Omega)]^d$ is abbreviated by $\|\cdot\|_{s,\Omega}$.

3 Finite element discretization

Let now $\mathcal{T}_h$ denote a simplicial triangulation of the domain Ω without hanging nodes. For each $T \in \mathcal{T}_h$, we define

$$h_T := \max_{f\subset\partial T} h_f,$$

with h_f the diameter of the face f. Moreover, we assume that the mesh is regular in the sense that

- (local shape regularity) for all simplices $T \in \mathcal{T}_h$ there holds

$$\frac{h_T}{\operatorname{diam}(T)} < C,$$

  where $\operatorname{diam}(T)$ means the diameter of the largest inscribed ball in T and C is a fixed constant;
- (local quasi uniformity) for any two elements $T, T' \in \mathcal{T}_h$ having at least one common node there holds $h_T < \rho h_{T'}$, with $\rho > 0$.

The mesh $\mathcal{T}_h$ will be called a macro triangulation and we derive a second triangulation $\tilde{\mathcal{T}}_h$ from $\mathcal{T}_h$. For each macro simplex $T \in \mathcal{T}_h$ we connect its barycenter with its vertices, in order to construct a new triangulation. In two space dimensions we get three triangles from each macro triangle and in three space dimensions we get four tetrahedra from each macro tetrahedron. This new triangulation $\tilde{\mathcal{T}}_h$ is locally shape regular and locally quasi uniform, although the constants for interpolation estimates are worse, because we get larger angles.

For the finite element discretization we define V_h^k as the space of continuous functions of piecewise polynomials of order $k \geq 1$

$$V_h^k := \left\{ v \in H_0^1(\Omega) : v_{|T} \in P_k(T), \text{for all } T \in \tilde{\mathcal{T}}_h \right\}.$$

By Q_h^l we refer to the space of discontinuous functions of piecewise polynomials of order $l \geq 1$

$$Q_h^l(\tilde{\mathcal{T}}_h) := \left\{ q \in L^2(\Omega) : q_{|T} \in P_l(T), \text{for all } T \in \tilde{\mathcal{T}}_h \right\}.$$

For $k \geq d$ velocities are approximated in the space $[V_h^k]^d$, and pressures are approximated in Q_h^{k-1}.

We assume, that there exist projection operators $\tilde{\pi}_{\mathrm{h}}$: $V^d \to [V_h^k]^d$, and π_{h}: $Q \to Q_h^{k-1}$, with optimal approximation properties

$$\begin{aligned} \|\mathbf{v} - \tilde{\pi}_{\mathrm{h}}(\mathbf{v})\|_{0,\Omega} &\lesssim h^{\min\{r,k+1\}} \|\mathbf{v}\|_{\min\{r,k+1\}} \\ \|\nabla(\mathbf{v} - \tilde{\pi}_{\mathrm{h}}(\mathbf{v}))\|_{0,\Omega} &\lesssim h^{\min\{r-1,k\}} \|\mathbf{v}\|_{\min\{r,k+1\}} \end{aligned} \tag{4}$$

for all $\mathbf{v} \in V^d \cap [H^r(\Omega)]^d$, $r \in \mathbb{N}$ and

$$\|q - \pi_{\mathrm{h}}(q)\|_{0,\Omega} \lesssim h^{\min\{s,k\}} \|q\|_{\min\{s,k\}} \tag{5}$$

for all $q \in Q \cap H^s(\Omega)$ and $s \in \mathbb{N}_0$. We let π_{h} be defined by the standard L^2-projection, whereas the properties of $\tilde{\pi}_{\mathrm{h}}$ depend on the stabilization operator under investigation. The projection $\tilde{\pi}_{\mathrm{h}}$ will be required to satisfy an orthogonality condition $(\mathbf{v} - \tilde{\pi}_{\mathrm{h}}(\mathbf{v}), \mathbf{z}_h) = 0$ for all $\mathbf{z}_h \in [Z_h]^d$ where $[Z_h]^d$ is a

discrete space that will be specified for each of the two stabilization methods in Section 5.

In the following we denote by $\mathbf{a}_h \in [V_h^k]^d$ some piecewise linear interpolant of $\mathbf{a}$ satisfying $\|\mathbf{a} - \mathbf{a}_h\|_{\infty,T} \leq h_T \|\mathbf{a}\|_{W^{1,\infty}(T)}$ for all $T \in \tilde{\mathcal{T}}_h$. Usually, we will have $\mathbf{a}_h \not\subset \mathbf{H}$. For the error analysis, we will use the following inverse estimate, which is valid for all $v \in P_k(T)$, $T \in \tilde{\mathcal{T}}_h$

$$h_T \|\nabla \mathbf{v}_h\|_{0,T} \lesssim \|\mathbf{v}_h\|_{0,T}. \tag{6}$$

The presented mixed finite element is the well-known Scott-Vogelius element. Since the triangulation is derived from a regular macro triangulation and since we assume $k \geq d$, this discretization is LBB-stable for a standard Galerkin discretization of the Stokes problem [1,27]. Discrete LBB-stability is equivalent to the existence of the Fortin interpolant [10], i.e. for all $\mathbf{v} \in V^d$ there is a $\pi_{\mathrm{F}}(\mathbf{v}) \in [V_h^k]^d$ such that

$$\forall q_h \in Q_h^{k-1} : b(q_h, \mathbf{v}) = b(q_h, \pi_{\mathrm{F}}(\mathbf{v})) \quad \wedge \quad \|\pi_{\mathrm{F}}(\mathbf{v})\|_{1,\Omega} \lesssim \|\mathbf{v}\|_{1,\Omega}. \tag{7}$$

Moreover, Scott-Vogelius elements have the important property

$$\nabla \cdot [V_h^k]^d \subset Q_h^{k-1}. \tag{8}$$

In the case $g = 0$ this enforces pointwise mass conservation for the standard Galerkin discretization of the Stokes problem. This can easily be derived, since standard weak mass conservation for the discrete Stokes solution $\mathbf{u}_h$ means that for all $q_h \in Q_h^{k-1}$ holds

$$(-\nabla \cdot \mathbf{u}_h, q_h) = 0.$$

Due to (8) we can choose the special test function $q_h := -\nabla \cdot \mathbf{u}_h$ and we have exact mass conservation in the L_2 sense. But since discrete solutions $\mathbf{u}_h$ are piecewise polynomial, we also get $\nabla \cdot \mathbf{u}_h = 0$ pointwise inside each simplex of the triangulation. As we shall see, this result holds also for the discrete Oseen problem.

In the following, we are especially interested in the lowest order case $k = d$, but of course we are not restricted to it. Denoting the product space $X_h^k := [V_h^k]^d \times Q_h^{k-1}$ we propose the following finite element method: find $(\mathbf{u}_h, p_h) \in X_h^k$ such that

$$\begin{aligned} A_h[(\mathbf{u}_h, p_h), (\mathbf{v}_h, q_h)] &= (f, \mathbf{v}_h) + (g, q_h), \\ \text{with } A_h[(\mathbf{u}_h, p_h), (\mathbf{v}_h, q_h)] &:= A[(\mathbf{u}_h, p_h), (\mathbf{v}_h, q_h)] \\ &\quad + \mathrm{S_h}(\mathbf{u}_h, \mathbf{v}_h) \end{aligned} \tag{9}$$

for all $(\mathbf{v}_h, q_h) \in X_h^k$.

Here, $\mathrm{S_h}(\cdot,\cdot)$ is an abstract stabilization operator that is needed in the case of dominant convection. For the abstract stabilization operator we postulate the following properties

- (linearity) for all $\mathbf{u}_h, \mathbf{v}_h, \mathbf{w}_h \in [V_h^k]^d$ and $\lambda, \mu \in \mathbb{R}$ we have

$$\mathrm{S_h}(\lambda \mathbf{u}_h + \mu \mathbf{v}_h, \mathbf{w}_h) = \lambda\, \mathrm{S_h}(\mathbf{u}_h, \mathbf{w}_h) + \mu\, \mathrm{S_h}(\mathbf{v}_h, \mathbf{w}_h); \tag{10}$$

- (symmetry) for all $\mathbf{u}_h, \mathbf{v}_h \in [V_h^k]^d$ we have

$$\mathrm{S_h}(\mathbf{u}_h, \mathbf{v}_h) = \mathrm{S_h}(\mathbf{v}_h, \mathbf{u}_h); \tag{11}$$

- (non-negativity) for all $\mathbf{u}_h \in [V_h^k]^d$ we have

$$\mathrm{S_h}(\mathbf{u}_h, \mathbf{u}_h) \geq 0; \tag{12}$$

- (boundedness) for all $\mathbf{u}_h \in [V_h^k]^d$ we have

$$|\mathrm{S_h}(\mathbf{u}_h, \mathbf{u}_h)|^{\frac{1}{2}} \lesssim h^{\frac{1}{2}} \|\mathbf{u}_h\|_{1,\Omega}; \tag{13}$$

- (weak consistency) for all $\mathbf{u} \in V^d \cap [H^r(\Omega)]^d$ with $r \geq 2$ we have

$$|\mathrm{S_h}(\tilde{\pi}_\mathrm{h}\, \mathbf{u}, \tilde{\pi}_\mathrm{h}\, \mathbf{u})|^{\frac{1}{2}} \lesssim h^{\min(r-\frac{1}{2}, k+\frac{1}{2})} \|\mathbf{u}\|_{\min(r,k+1)}; \tag{14}$$

- (stability) there exists a quasi interpolation operator $\tilde{\pi}_\mathrm{h}^*\colon [Q_h^{k-1}(\tilde{\mathcal{T}}_h)]^d \to [Z_h]^d$ such that for all $\mathbf{v}_h \in [V_h^k]^d$, $\mathbf{w} \in V^d$ there holds

$$\begin{gathered}(\mathbf{w} - \tilde{\pi}_\mathrm{h}(\mathbf{w}), \tilde{\pi}_\mathrm{h}^*(\mathbf{a}_h \cdot \nabla \mathbf{v}_h)) = 0, \\ \|h^{\frac{1}{2}}(\mathbf{a}_h \cdot \nabla \mathbf{v}_h - \tilde{\pi}_\mathrm{h}^*(\mathbf{a}_h \cdot \nabla \mathbf{v}_h))\|_{0,\Omega} \lesssim |\mathrm{S_h}(\mathbf{v}_h, \mathbf{v}_h)|^{\frac{1}{2}}.\end{gathered} \tag{15}$$

Lemma 1 (Cauchy-Schwarz for the stabilization operator) *For the stabilization operator holds for all* $\mathbf{u}, \mathbf{v} \in V^d$

$$|\mathrm{S_h}(\mathbf{u}_h, \mathbf{v}_h)| \leq [\mathrm{S_h}(\mathbf{u}_h, \mathbf{u}_h)]^{\frac{1}{2}}\, [\mathrm{S_h}(\mathbf{v}_h, \mathbf{v}_h)]^{\frac{1}{2}}\,. \tag{16}$$

PROOF. See the classical proof for scalar products. There, the properties (10), (11) and (12) are needed.

4 A priori error analysis

In the following a priori convergence analysis we investigate the convergence behavior of the proposed method depending on higher regularity assumptions and the parameters $\{\nu, \alpha, \mathbf{a}\}$.

For the analysis we introduce the following energy scalar product for all $\mathbf{u}, \mathbf{v} \in V^d$

$$(\mathbf{u}, \mathbf{v})_e := \nu(\nabla \mathbf{u}, \nabla \mathbf{v}) + \alpha(\mathbf{u}, \mathbf{v})$$

The corresponding energy norm is denoted by $\|\cdot\|_e$. Further, we introduce the following triple norm for all $(\mathbf{u}, p) \in X$

$$|||(\mathbf{u}, p)|||^2 := \|\mathbf{u}\|_e^2 + \|\nabla \cdot \mathbf{u}\|_{0,\Omega}^2 + \|p\|_{0,\Omega}^2.$$

and a mesh-dependent discrete counterpart for all $(\mathbf{u}_h, p_h) \in X_h^k$ accounting also for the size of the stabilization term

$$|||(\mathbf{u}_h, p_h)|||_h^2 := \|\mathbf{u}_h\|_e^2 + \|\nabla \cdot \mathbf{u}_h\|_{0,\Omega}^2 + [\mathrm{S_h}(\mathbf{u}_h, \mathbf{u}_h)] + \|p_h\|_{0,\Omega}^2.$$

Lemma 2 (coercivity) *For all $\mathbf{u} \in V^d$, $p \in Q$ we have the following coercivity property*

$$A_h[(\mathbf{u}, p), (\mathbf{u}, -p - \nabla \cdot \mathbf{u})] = |||(\mathbf{u}, 0)|||_h^2.$$

PROOF. The proof follows from the anti-symmetry of the convective term, since $\nabla \cdot \mathbf{a} = 0$ holds.

Lemma 3 (weak consistency) *Let $(\mathbf{u}, p)$ be the solution of (2) and let $(\mathbf{u}_h, p_h)$ be the solution of (9) then*

$$A[(\mathbf{u} - \mathbf{u}_h, p - p_h), (\mathbf{v}_h, q_h)] = \mathrm{S_h}(\mathbf{u}_h, \mathbf{v}_h).$$

PROOF. The lemma is obtained by subtracting (9) from (2).

Lemma 4 (Young) *for all $a, b \geq 0$ and $\epsilon > 0$ we have*

$$ab \leq \frac{1}{2\epsilon} a^2 + \frac{\epsilon}{2} b^2.$$

Lemma 5 *Suppose $\mathbf{u} \in V^d \cap H^r(\Omega)$, $r \geq 2$ and suppose that $[V_h^k]^d$ is a piecewise polynomial space with $k \geq d$, then there holds*

$$|||(\mathbf{u} - \tilde{\pi}_\mathrm{h}(\mathbf{u}), 0)||| + S_h(\tilde{\pi}_\mathrm{h}(\mathbf{u}), \tilde{\pi}_\mathrm{h}(\mathbf{u}))^{\frac{1}{2}} \lesssim \left(\nu^{\frac{1}{2}} + \alpha^{\frac{1}{2}} h + h^0 + h^{\frac{1}{2}}\right) h^{\min(r-1,k)} \times \|\mathbf{u}\|_{\min(r,k+1)}. \tag{17}$$

PROOF. The lemma is proven by applying (4) and (14).

Lemma 6 *Suppose* $\mathbf{u} \in V^d \cap H^r(\Omega)$, $r \geq 2$, $p \in Q \cap H^s(\Omega)$, $s > 0$ *and suppose that* $[V_h^k]^d$ *is a piecewise polynomial velocity space with* $k \geq d$ *and* Q_h^{k-1} *is the corresponding pressure space , then there holds*

$$\begin{aligned} |||(\mathbf{u} - \tilde{\pi}_{\mathrm{h}}(\mathbf{u}), p - \pi_{\mathrm{h}}(p))||| + S_h(\tilde{\pi}_{\mathrm{h}}(\mathbf{u}), \tilde{\pi}_{\mathrm{h}}(\mathbf{u}))^{\frac{1}{2}} \lesssim \Big(\Big(\nu^{\frac{1}{2}} + \alpha^{\frac{1}{2}} h + h^0 + h^{\frac{1}{2}} \Big) \\ \times h^{\min(r-1,k)} \|\mathbf{u}\|_{\min(r,k+1)} \\ + h^{\min(s,k)} \|p\|_{\min(s,k)} \Big), \end{aligned} \tag{18}$$

PROOF. See lemma 5 and (5).

Theorem 7 (stability) *The stabilized finite element method in (9) satisfies the following stability property. For all* $(\mathbf{u}_h, p_h) \in X_h^k$ *with* $k \geq d$ *there holds*

$$c_S |||(\mathbf{u}_h, p_h)|||_h \leq \sup_{\substack{(\mathbf{v}_h, q_h) \in X_h^k, \\ |||(\mathbf{v}_h, q_h)||| \neq 0}} \frac{A_h[(\mathbf{u}_h, p_h), (\mathbf{v}_h, q_h)]}{|||(\mathbf{v}_h, q_h)|||_h}. \tag{19}$$

Here, the constant c_S *is independent of the mesh size and does not degenerate as* $\nu \to 0$.

PROOF. By the discrete LBB-stability we find $\mathbf{v}_{p_h} \in V^d$ such that $\nabla \cdot \mathbf{v}_{p_h} = p_h$, $\nabla \cdot (\pi_{\mathrm{F}}(\mathbf{v}_{p_h})) = p_h$, $\|\mathbf{v}_{p_h}\|_{1,\Omega} \lesssim \|p_h\|_{0,\Omega}$ and $\|\pi_{\mathrm{F}}(\mathbf{v}_{p_h})\|_{1,\Omega} \lesssim \|p_h\|_{0,\Omega}$.

Taking $(\mathbf{v}_h, q_h) = (-\pi_{\mathrm{F}}(\mathbf{v}_{p_h}), p_h)$, we compute

$$\begin{aligned} A_h[(\mathbf{u}_h, p_h), (-\pi_{\mathrm{F}}(\mathbf{v}_{p_h}), p_h)] \geq \|p_h\|_{0,\Omega}^2 \\ - \nu \|\nabla \mathbf{u}_h\|_{0,\Omega} \|\nabla \pi_{\mathrm{F}}(\mathbf{v}_{p_h})\|_{0,\Omega} - \alpha \|\mathbf{u}_h\|_{0,\Omega} \|\pi_{\mathrm{F}}(\mathbf{v}_{p_h})\|_{0,\Omega} \\ - \|\mathbf{u}_h\|_{0,\Omega} \|\mathbf{a}\|_{L^\infty(\Omega)} \|\nabla \pi_{\mathrm{F}}(\mathbf{v}_{p_h})\| - \|\nabla \cdot \mathbf{u}_h\|_{0,\Omega} \|p_h\|_{0,\Omega} \\ - [\mathrm{S_h}(\mathbf{u}_h, \mathbf{u}_h)]^{\frac{1}{2}} [\mathrm{S_h}(\pi_{\mathrm{F}}(\mathbf{v}_{p_h}), \pi_{\mathrm{F}}(\mathbf{v}_{p_h}))]^{\frac{1}{2}}. \end{aligned}$$

We conclude using the stability properties of $\mathbf{v}_{p_h}$ and $\pi_{\mathrm{F}}(\mathbf{v}_{p_h})$ and by the boundedness of the stabilization operator (13)

$$\begin{aligned} \|\pi_{\mathrm{F}}(\mathbf{v}_{p_h})\|_{0,\Omega} &\lesssim \|p_h\|_{0,\Omega}, \\ \|\nabla \pi_{\mathrm{F}}(\mathbf{v}_{p_h})\|_{0,\Omega} &\lesssim \|p_h\|_{0,\Omega}, \\ [\mathrm{S_h}(\pi_{\mathrm{F}}(\mathbf{v}_{p_h}), \pi_{\mathrm{F}}(\mathbf{v}_{p_h}))]^{\frac{1}{2}} &\lesssim h^{\frac{1}{2}} \|p_h\|_{0,\Omega}. \end{aligned} \tag{20}$$

For each of the five negative terms in the right hand side of the inequality we

use Lemma 4 with some $\epsilon > 0$, which is to be determined. We get

$$\begin{aligned} A_h[(\mathbf{u}_h, p_h), (-\pi_{\mathrm{F}}(\mathbf{v}_{p_h}), p_h)] \gtrsim \|p_h\|_{0,\Omega}^2 - \\ \frac{1}{2\epsilon}(\nu\|\nabla \mathbf{u}_h\|_{0,\Omega}^2 + \alpha\|\mathbf{u}_h\|_{0,\Omega}^2 + \|\nabla\cdot\mathbf{u}_h\|_{0,\Omega}^2 \\ + \mathrm{S_h}(\mathbf{u}_h, \mathbf{u}_h) + \|\mathbf{a}\|_{L^\infty}\|\mathbf{u}_h\|_{0,\Omega}^2) \\ - \frac{\epsilon}{2}(\nu + \alpha + 1 + \|\mathbf{a}\|_{L^\infty} + 1)\,\|p_h\|_{0,\Omega}^2. \end{aligned}$$

Now we set

$$\epsilon^{-1} := 2 + \nu + \alpha + \|\mathbf{a}\|_{L^\infty}$$

and have

$$\begin{aligned} A_h[(\mathbf{u}_h, p_h), (-\pi_{\mathrm{F}}(\mathbf{v}_{p_h}), p_h)] &\gtrsim \tfrac{1}{2}\|p_h\|_{0,\Omega}^2 \\ &\quad - \frac{1}{2\epsilon}(\nu\|\nabla\mathbf{u}_h\|_{0,\Omega}^2 + (\alpha + \|\mathbf{a}\|_{L^\infty})\|\mathbf{u}_h\|_{0,\Omega}^2 \\ &\quad + \ \|\nabla\cdot\mathbf{u}_h\|_{0,\Omega}^2 + \mathrm{S_h}(\mathbf{u}_h, \mathbf{u}_h)) \\ &\gtrsim \tfrac{1}{2}\|p_h\|_{0,\Omega}^2 \ - \frac{1}{2\epsilon}(1 + \frac{\|\mathbf{a}\|_{L^\infty}}{\alpha})|\!|\!|(\mathbf{u}_h, 0)|\!|\!|_h^2. \end{aligned}$$

Setting

$$M := \epsilon^{-1}(1 + \frac{\|\mathbf{a}\|_{L^\infty}}{\alpha}) = (2 + \nu + \alpha + \|\mathbf{a}\|_{L^\infty})(1 + \frac{\|\mathbf{a}\|_{L^\infty}}{\alpha})$$

we finally have

$$A_h[(\mathbf{u}_h, p_h), (-\pi_{\mathrm{F}}(\mathbf{v}_{p_h}), p_h)] \gtrsim \tfrac{1}{2}\|p_h\|_{0,\Omega}^2 - \frac{M}{2}|\!|\!|(\mathbf{u}_h, 0)|\!|\!|_h^2.$$

Now we choose

$$\begin{aligned} (\mathbf{v}_h, q_h) &:= (\mathbf{u}_h - \frac{2}{1+M}\,\pi_{\mathrm{F}}(\mathbf{v}_{p_h}), \frac{1-M}{1+M}p_h - \nabla\cdot\mathbf{u}_h) \\ &= (\mathbf{u}_h, -p_h - \nabla\cdot\mathbf{u}_h) + \frac{2}{1+M}(-\pi_{\mathrm{F}}(\mathbf{v}_{p_h}), p_h) \end{aligned}$$

and get immediately by lemma 2 and the previous calculation

$$A_h[(\mathbf{u}_h, p_h), (\mathbf{v}_h, q_h)] \gtrsim \frac{1}{1+M}|\!|\!|(\mathbf{u}_h, p_h)|\!|\!|_h^2.$$

We end the proof by showing that $|\!|\!|(\mathbf{v}_h, q_h)|\!|\!|_h \lesssim |\!|\!|(\mathbf{u}_h, p_h)|\!|\!|_h$. Therefore, we use the triangle inequality for the triple norm and apply the three estimates

in (20)

$$\begin{aligned}
|\!|\!|(\mathbf{v}_h, q_h)|\!|\!|_h &\leq |\!|\!|(\mathbf{u}_h, -p_h)|\!|\!|_h + |\!|\!|(0, -\nabla\cdot\mathbf{u}_h)|\!|\!|_h + \frac{2}{1+M}|\!|\!|(-\pi_{\mathrm{F}}(\mathbf{v}_{p_h}), p_h)|\!|\!|_h \\
&\lesssim 2|\!|\!|(\mathbf{u}_h, p_h)|\!|\!|_h + \frac{2}{1+M}(3^{\frac{1}{2}} + \nu^{\frac{1}{2}} + \alpha^{\frac{1}{2}})\|p_h\|_{0,\Omega} \\
&\lesssim (1 + \nu^{\frac{1}{2}} + \alpha^{\frac{1}{2}})|\!|\!|(\mathbf{u}_h, p_h)|\!|\!|_h.
\end{aligned}$$

We conclude

$$\frac{A_h[(\mathbf{u}_h, p_h), (\mathbf{v}_h, q_h)]}{|\!|\!|(\mathbf{u}_h, p_h)|\!|\!|_h |\!|\!|(\mathbf{v}_h, q_h)|\!|\!|_h} \gtrsim \frac{1}{1+M}\frac{1}{1 + \nu^{\frac{1}{2}} + \alpha^{\frac{1}{2}}}$$

If we assume that $\nu \ll 1$ and $\|\mathbf{a}\|_{L^\infty} = \mathcal{O}(1)$, we get $c_S \approx \mathcal{O}(\min\{\alpha, \alpha^{-\frac{3}{2}}\})$. In particular, the estimate is independent from the mesh size.

Remark 8 *The estimate on c_S indicates instability for $\alpha \to 0$. This behavior cannot be seen in numerical experiments. On the other hand it is known also in the case of scalar advection-diffusion-reaction equations. In that case one may improve the analysis using exponentially weighted test functions as proposed in [20]. Such an analysis is beyond the scope of the present paper.*

Theorem 9 (a priori error estimate) *Let $(\mathbf{u}, p)$ be the solution of (2) and $(\mathbf{u}_h, p_h)$ be the solution of (9) then, under the same assumptions on the regularity of $\mathbf{u}$ and p as for Lemma 6, there holds*

$$\begin{aligned}
|\!|\!|(\mathbf{u} - \mathbf{u}_h, p - p_h)|\!|\!| \lesssim\ & h^{\min(r-1,k)}\|\mathbf{u}\|_{\min(r,k+1)} \\
& + h^{\min(s,k)}\|p\|_{\min(s,k)}.
\end{aligned} \tag{21}$$

In addition, for the velocities alone we have the result

$$|\!|\!|(\mathbf{u} - \mathbf{u}_h, 0)|\!|\!| + S_h(\mathbf{u}_h, \mathbf{u}_h)^{\frac{1}{2}} \lesssim h^{\min(r-1,k)}\|\mathbf{u}\|_{\min(r,k+1)}, \tag{22}$$

where the approximation order of the discrete velocities is independent from the pressure regularity.

PROOF. In the general case we start using the triangle inequality for the triple norm

$$\begin{aligned}
|\!|\!|(\mathbf{u} - \mathbf{u}_h, p - p_h)|\!|\!| \leq\ & |\!|\!|(\mathbf{u} - \tilde{\pi}_{\mathrm{h}}(\mathbf{u}), p - \pi_{\mathrm{h}}(p)|\!|\!| \\
& + |\!|\!|(\mathbf{u}_h - \tilde{\pi}_{\mathrm{h}}(\mathbf{u}), p_h - \pi_{\mathrm{h}}(p))|\!|\!|_h.
\end{aligned}$$

The first term in the second line can be estimated immediately by lemma 6.

In order to obtain the estimate (22) we simply start the analysis with

$$\begin{aligned}|\!|\!|(\mathbf{u}-\mathbf{u}_h,0)|\!|\!| &\leq |\!|\!|(\mathbf{u}-\mathbf{u}_h,\pi_{\mathrm{h}}(p)-p_h)|\!|\!| \\ &\leq |\!|\!|(\mathbf{u}-\tilde{\pi}_{\mathrm{h}}(\mathbf{u}),0)|\!|\!| + |\!|\!|(\mathbf{u}_h-\tilde{\pi}_{\mathrm{h}}(\mathbf{u}),p_h-\pi_{\mathrm{h}}(p))|\!|\!|_h.\end{aligned} \tag{23}$$

Similar to the previous case we can estimate the first term of the second line by lemma 5. We then apply theorem 7 to the second term, which is identical in both cases. Introducing the discrete errors $\xi_h^{\mathbf{u}} := \mathbf{u}_h - \tilde{\pi}_{\mathrm{h}}(\mathbf{u})$ and $\xi_h^p := p_h - \pi_{\mathrm{h}}(p)$ we have

$$c_S|\!|\!|(\xi_h^{\mathbf{u}},\xi_h^p)|\!|\!|_h \leq \sup_{\substack{(\mathbf{v}_h,q_h)\in X_h^k,\\ |\!|\!|(\mathbf{v}_h,q_h)|\!|\!|_h\neq 0}} \frac{A_h[(\xi_h^{\mathbf{u}},\xi_h^p),(\mathbf{v}_h,q_h)]}{|\!|\!|(\mathbf{v}_h,q_h)|\!|\!|_h}.$$

Now we investigate the numerator of the fraction on the right hand side. By weak consistency in lemma 3 and the Cauchy-Schwarz inequality we get

$$\begin{aligned}|A_h[(\xi_h^{\mathbf{u}},\xi_h^p),(\mathbf{v}_h,q_h)]| &= |A[(\mathbf{u}-\tilde{\pi}_{\mathrm{h}}(\mathbf{u}),p-\pi_{\mathrm{h}}(p)),(\mathbf{v}_h,q_h)] - \mathrm{S_h}(\tilde{\pi}_{\mathrm{h}}(\mathbf{u}),\mathbf{v}_h)| \\ &\leq |\!|\!|(\mathbf{u}-\tilde{\pi}_{\mathrm{h}}(\mathbf{u}),0)|\!|\!||\!|\!|(\mathbf{v}_h,0)|\!|\!| \\ &\quad + |(\mathbf{u}-\tilde{\pi}_{\mathrm{h}}(\mathbf{u}),\mathbf{a}\cdot\nabla\mathbf{v}_h)| \\ &\quad + |(p-\pi_{\mathrm{h}}(p),\nabla\cdot\mathbf{v}_h)| + |(q_h,\nabla\cdot(\mathbf{u}-\tilde{\pi}_{\mathrm{h}}(\mathbf{u})))| \\ &\quad + [\mathrm{S_h}(\tilde{\pi}_{\mathrm{h}}(\mathbf{u}),\tilde{\pi}_{\mathrm{h}}(\mathbf{u}))]^{\frac{1}{2}}[\mathrm{S_h}(\mathbf{v}_h,\mathbf{v}_h)]^{\frac{1}{2}}.\end{aligned} \tag{24}$$

First note that by the orthogonality of the L^2-projection we have

$$|(p-\pi_{\mathrm{h}}(p),\nabla\cdot\mathbf{v}_h)| = 0$$

so the only term involving the projection error of the pressure vanishes. Since the L^2-norm of the pressure and the divergence are included in the triple norm, we can conclude

$$\begin{aligned}|A_h[(\xi_h^{\mathbf{u}},\xi_h^p),(\mathbf{v}_h,q_h)]| &\lesssim |\!|\!|(\mathbf{u}-\tilde{\pi}_{\mathrm{h}}(\mathbf{u}),0)|\!|\!||\!|\!|(\mathbf{v}_h,q_h)|\!|\!| \\ &\quad + |(\mathbf{u}-\tilde{\pi}_{\mathrm{h}}(\mathbf{u}),\mathbf{a}\cdot\nabla\mathbf{v}_h)| \\ &\quad + [\mathrm{S_h}(\tilde{\pi}_{\mathrm{h}}(\mathbf{u}),\tilde{\pi}_{\mathrm{h}}(\mathbf{u}))]^{\frac{1}{2}}|\!|\!|(\mathbf{v}_h,0)|\!|\!|_h.\end{aligned}$$

The second term on the right hand side is estimated as follows. We use the triangle inequality, the stability property of the stabilization operator (15) and the inverse estimate (6).

$$\begin{aligned}|(\mathbf{u}-\tilde{\pi}_{\mathrm{h}}(\mathbf{u}),\mathbf{a}\cdot\nabla\mathbf{v}_h)| &\leq |(\mathbf{u}-\tilde{\pi}_{\mathrm{h}}(\mathbf{u}),(\mathbf{a}-\mathbf{a}_h)\cdot\nabla\mathbf{v}_h)| \\ &\quad + |(\mathbf{u}-\tilde{\pi}_{\mathrm{h}}(\mathbf{u}),\mathbf{a}_h\cdot\nabla\mathbf{v}_h - \tilde{\pi}_{\mathrm{h}}^*(\mathbf{a}_h\cdot\nabla\mathbf{v}_h))| \\ &\lesssim \|\mathbf{a}\|_{W^{1,\infty}}\alpha^{-\frac{1}{2}}\|\mathbf{u}-\tilde{\pi}_{\mathrm{h}}(\mathbf{u})\|_{0,\Omega}\,\mathrm{S_h}(\mathbf{v}_h,\mathbf{v}_h) \\ &\quad + \|h^{-\frac{1}{2}}(\mathbf{u}-\tilde{\pi}_{\mathrm{h}}(\mathbf{u}))\|_{0,\Omega}|\!|\!|(\mathbf{v}_h,0)|\!|\!|_h.\end{aligned}$$

Altogether, with lemma 6 we have the following estimate

$$|||(\xi_h^{\mathbf{u}}, \xi_h^p)||| \lesssim \frac{1}{c_S}\{(\nu^{\frac{1}{2}} + (\alpha^{-\frac{1}{2}} + \alpha^{\frac{1}{2}})h + h^0 + h^{\frac{1}{2}})h^{\min(r-1,k)}\|\mathbf{u}\|_{\min(r,k+1)} + h^{\min(s,k)}\|p\|_{\min(s,k)} + h^{\min(r-\frac{1}{2},k+\frac{1}{2})}\|\mathbf{u}\|_{\min(r,k+1)}\}.$$

The first error estimate is now derived with a constant $c \approx \max\{\mathcal{O}(\alpha^{-1}, \alpha^{\frac{3}{2}})\}$.

In the special case $g = 0$ the discrete solution $\mathbf{u}_h$ lies in the space $\mathbf{H}$ and is completely decoupled from the pressure.

Remark 10 *The a priori error estimate does not allow us to conclude that convergence improves in the L^2-norm thanks to the stabilization operator. This is due to the fact that the contribution of the divergence of the solution dominates the error estimate in the case of high Reynolds numbers. Also note that even in case $g = 0$ it does not seem possible to prove optimal estimates thanks to the stabilization. In the numerical section we show in a linear example that the stabilized method can lead to smaller error in both L^2- and H^1-norms. Then in a non-linear example we show that the stabilization damps spurious oscillations on coarse meshes.*

5 Two stabilization operators

In the following we present two different stabilization operators, that enter the abstract framework proposed above. Other methods such as the orthogonal subscales proposed by Codina, [9] or the subgrid viscosity method proposed by John and Kaya [18] could also be considered. An overview of some recent stabilization methods for the Oseen's equation is given in [4].

5.1 Edge/face stabilization

The edge/face stabilization was analyzed for the first time in [7] for finite element discretizations of convection-diffusion-reaction equations. Later, the method was extended to incompressible flow problems [5]. The stabilization operator reads as

$$\mathrm{S_h}(\mathbf{u}, \mathbf{v}) = \sum_{T \in \tilde{\mathcal{T}}_h} \tfrac{1}{2} \int_{\partial T} \gamma h_{\partial T}^2 [\nabla \mathbf{u}] \cdot [\nabla \mathbf{v}] \, \mathrm{d}s. \tag{25}$$

Here, $h_{\partial T}$ is the size of ∂T, $[q]$ denotes the jump of q across ∂T for $\partial T \cap \partial\Omega = \emptyset$, $[q] = 0$ on $\partial T \cap \partial\Omega \neq \emptyset$ and γ is a tuning parameter.

For this operator we see (10)–(13) at once. Also (14) is easily verified, since for functions $\mathbf{u} \in [H^2(\Omega)]^d$ the trace of $\nabla \mathbf{u}$ is well defined and the stabilization vanishes. Therefore, face stabilization is H^2-consistent. For the remaining features of the stabilization we refer the reader to [7,5]. Here, the operator $\tilde{\pi}_{\mathrm{h}}$ is defined by the standard L^2-projection onto the space $[Z_h]^d := [V_h^k]^d$ and $\tilde{\pi}_{\mathrm{h}}^* : [Q_h^{k-1}(\tilde{\mathcal{T}}_h)]^d \to [Z_h]^d$ is defined by the Oswald-quasi interpolation operator defined in each node x_i as the straight average

$$\tilde{\pi}_{\mathrm{h}}^* u(x_i) = \frac{1}{n_i} \sum_{\{K : x_i \in K\}} u(x_i)|_k$$

where n_i denotes the number of triangles sharing node x_i. One may then show that the stabilization term (25) satisfies also the condition (15). A streamline-diffusion type operator is obtained by choosing $\gamma = \gamma_0 |\mathbf{a} \cdot n_{\partial T}|$. For details see [5].

5.2 Local projection stabilization

The local projection method was introduced in [2] and was analyzed for the Oseen's problem in [3]. In order to define the method we define the space of discontinuous functions on the macroelement mesh and set $Z_h := [Q_h^{k-1}(\mathcal{T}_h)]^d$. It is a discontinuous finite element space of order $k-1$, which is continuous over the macro simplices of the macro triangulation $\mathcal{T}_h$. With the (local) L_2-projection $\bar{\pi}_{h,k-1} : [Q_h^{k-1}(\tilde{\mathcal{T}}_h)]^d \to [Z_h]^d$ we define the following fluctuation operator

$$\bar{\kappa}_h := I - \bar{\pi}_{h,k-1}, \tag{26}$$

where I stands for the identity mapping. Now the convection is stabilized by

$$\mathrm{S_h}(\mathbf{u}, \mathbf{v}) = (\gamma |a| h_T \bar{\kappa} \nabla \mathbf{u}, \bar{\kappa} \nabla \mathbf{v}). \tag{27}$$

Again, we can directly see that (10), (11), and (12) are valid for this operator. In the abstract setting above $\tilde{\pi}_{\mathrm{h}}^*$ is given by the operator $\bar{\pi}_{h,k-1}$. The corresponding projector $\tilde{\pi}_{\mathrm{h}}$ is defined as a variant of the Scott-Zhang interpolation as defined in [24] modified to satisfy the orthogonality constraint of (15). For details on the analysis we refer to [3].

6 Numerical examples

In this section we illustrate the theoretical results obtained above with two computational experiments. All numerical computations are performed using the finite element toolbox ALBERTA [23]. The evolving sparse linear systems are solved by the efficient direct solver PARDISO [14,22].

6.1 A linear example

First, we consider the linear problem (1) in the two dimensional case. We approximate the following continuous solution $\mathbf{u} = (u, v)$ in the domain $\Omega = [0,1] \times [0,1]$. The example was taken from [13] and slightly modified.

$$\begin{aligned} \psi(x,y) &= c_1 x^2 (x-1)^2 y^2 (y-1)^2 \\ u(x,y) &= \partial_y \psi \\ v(x,y) &= -\partial_x \psi \\ p(x,y) &= c_2 (x^3 + y^3 - \tfrac{1}{2}). \end{aligned}$$

We choose $\nu = 10^{-4}$, $\alpha = 100 \cdot 2\pi^2 \nu \approx 0.197392$, $\mathbf{a} = \mathbf{u}$, $c_1 = 256$, $c_2 = 21.03485$ and compute the resulting right hand side $\mathbf{f}$. Here, the parameter α corresponds to a rough estimate for the time step in an instationary scheme for computing the asymptotic limit $t \to \infty$ in a fictitious time-dependent Oseen problem. The chosen parameter is related to the smallest eigenvalue of the Laplace operator and therefore allows to resolve the dissipation of energy in the equation. By the choice of the parameter c_2 the rotation and the divergence part of the (smooth) right hand side $\mathbf{f}$ are balanced. Therefore, quite a big pressure gradient is guaranteed and non-solenoidal discretizations will produce velocity approximations, which are polluted by bad approximation of the continous pressure.

For this numerical test problem we compare three different discretizations: the Galerkin Taylor-Hood element $P_2 - P_1$ (GTH), the Galerkin Scott-Vogelius element $P_2 - P_{-1}$ (GSV) and the stabilized Scott-Vogelius element with stabilization parameter

$$\gamma = \gamma_0 \|\mathbf{a}\|_{0,\Omega}^2 \tag{28}$$

and stabilization parameter $\gamma_0 = 3.085 \cdot 10^{-3}$. The parameter is tuned by minimizing the error on the coarsest mesh. All the computations are performed on macro element meshes as described above, which are derived from a uniform triangulation of the unit square, see figure 1. For the first numerical example we used 4 consecutive meshes, with $N = 16, 32, \ldots, 128$ elements on each side of the unit square. We present the velocity errors in the L_2 and the H_1 norm. The pressure error is presented in the L_2 norm. For the first test case we note the following approximate convergence orders for the stabilized Scott-Vogelius element:

- $\|\mathbf{u} - \mathbf{u}_h\|_{0,\Omega} \lesssim h^{3.29}$
- $\|\nabla(\mathbf{u} - \mathbf{u}_h)\|_{0,\Omega} \lesssim h^{2.25}$
- $\|p - p_h\|_{0,\Omega} \lesssim h^{2.05}$
- $|||\mathbf{u} - \mathbf{u}_h|||_h \lesssim h^{2.44}$.

The corresponding convergence behavior is shown in figures 2 and 3.

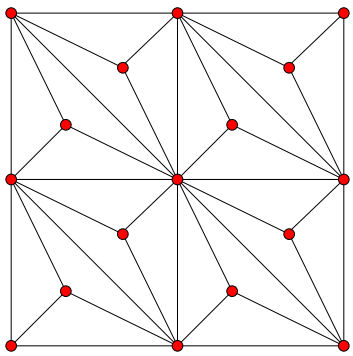

Fig. 1. Macro Element Triangulation of the Unit Square. $N = 2$

We recognize that the error of the stabilized Scott-Vogelius solution is smaller

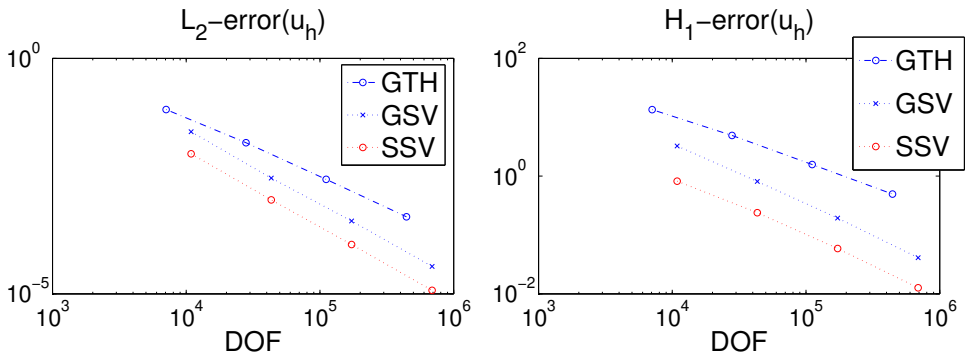

Fig. 2. Comparison between Galerkin Taylor-Hood (GTH), Galerkin Scott-Vogelius (GSV) and stabilized Scott-Vogelius (SSV), velocities

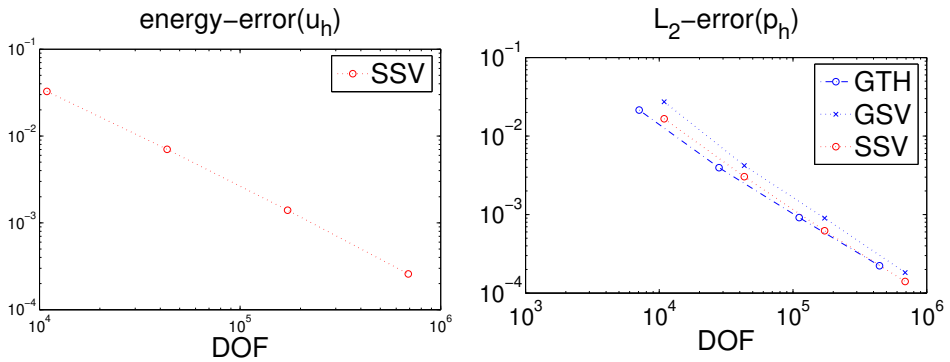

Fig. 3. Comparison between Galerkin Taylor-Hood (GTH), Galerkin Scott-Vogelius (GSV) and stabilized Scott-Vogelius (SSV), velocities and pressure

than that of its Galerkin counterpart on the computational meshes considered, about one half refinement step in the L_2 norm and one refinement step in the H_1 norm. The superior performance of the Scott-Vogelius element compared to

the standard Taylor-Hood elements for the velocity approximations is clearly visible in figure 2.

6.2 A nonlinear example - driven cavity in two dimensions

As a second example, we present numerical computations for the Navier-Stokes equation. We choose the well-known driven cavity problem in two space dimensions at Reynolds number 5000 and prescribe the velocity $\mathbf{u} = (1, 0)$ at the top of the cavity and no-slip boundary conditions elsewhere. At this Reynolds number the steady state solution is stable and reference solutions for comparison are available in the literature (see [16,11]).

By computing the asymptotic limit for $t \to \infty$, we have approximated numerically this stable steady solution. In this situation, the fully implicit backward Euler method is sufficient as time discretization scheme. We start from Stokes solutions and increase the time step manually during the computation. The nonlinear system is solved by a simple, undamped fixed point iteration.

Discretization in space is performed by the quadratic Scott-Vogelius element, similar to the linear example above. We compare the corresponding Galerkin discretization (GSV-N) to a stabilized formulation with the classical linear edge stabilization (SSV-N) on a sequence of four uniform macro element meshes. On the coarsest grid ($N = 8$) we get $2 \cdot 8 \cdot 8 = 128$ macro elements and about 450 divergence-free ansatz functions in the approximation space. For the stabilized method we here choose $\gamma = 4.0 \cdot 10^{-3}$ as stabilization parameter.

In figure 4 we show the stabilized solution on the finest grid with $N = 64$. Here, we can see the typical picture of the continuous solution quite well. There are two secondary vortices in the bottom corner and a third one in the upper left corner. In addition, also the small tertiary vortex in the lower right corner is resolved. The numerical results compare well to the data given e.g. in [16].

While the Galerkin discretization seems to be quite stable on the finest grid and hardly differs there from the stabilized solution, we expect pronounced spurious oscillations in the Galerkin solution on coarse grids due to the non-dissipative approximation of the first-order derivate. Such oscillations can easily made visible by plotting the velocity-components of the Galerkin solution on straight lines through the cavity.

First, we demonstrate in figure 5 that the Galerkin (GSV-64) and the stabilized discretization (SSV-64) do not differ much on the finest grid. Even on this fine grid the standard Galerkin method presents spurious oscillations although

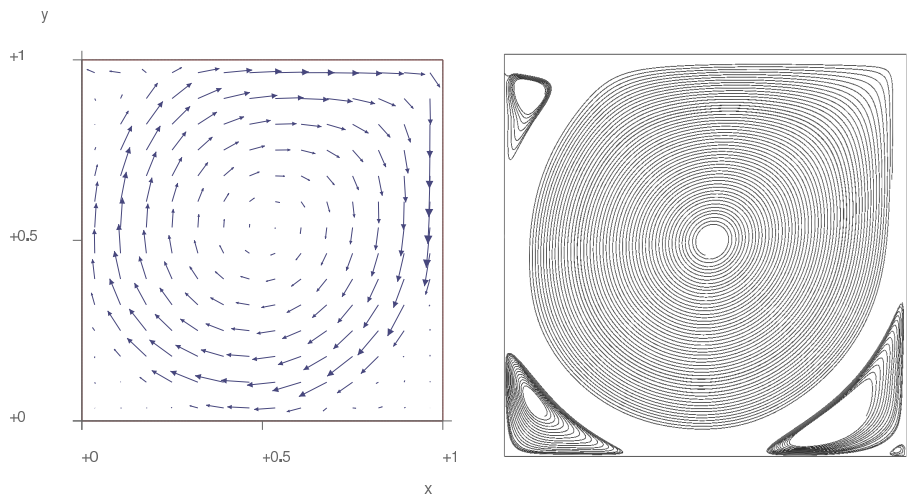

Fig. 4. Driven cavity at Reynolds number 5000 using the SSV-64 discretization. First picture: Velocity field. Second picture: Five numerical trajectories in the velocity field beginning at the following points: $(0.1, 0.9)$, $(0.1, 0.1)$, $(0.9, 0.1)$, $(0.5, 0.5)$, $(0.978, 0.022)$

their amplitude is very small. The influence of the grid resolution on the

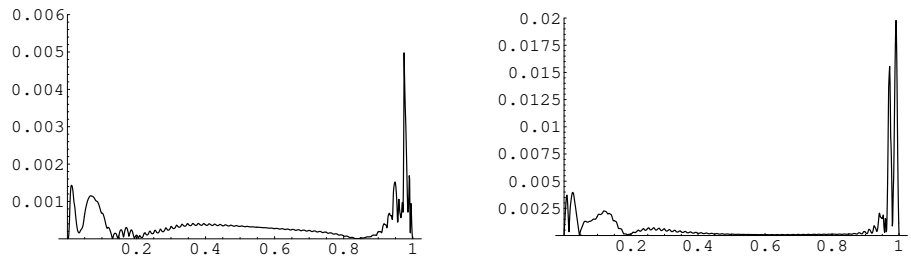

Fig. 5. Absolute Values of the Difference between GSV-64 and SSV-64 discretizations on the straight line $y = 0.9$. First picture: difference of u-components. Second picture: difference of v-components

Galerkin and the stabilized discretization can be studied in figures 6 and 7. As expected, in the stabilized discretization spurious oscillations are reduced in comparison to the Galerkin discretization. However, it is not clear from these graphics that the solution quality actually improves in the L^2-norm when adding the stabilization terms. For the straight lines $x = 0.5$ and $y = 0.5$ we can find some reference values for the u and v components in the literature. In figures 8 and 9, the results are compared to a reference solution presented in [11]. The reference values are visualized by points.

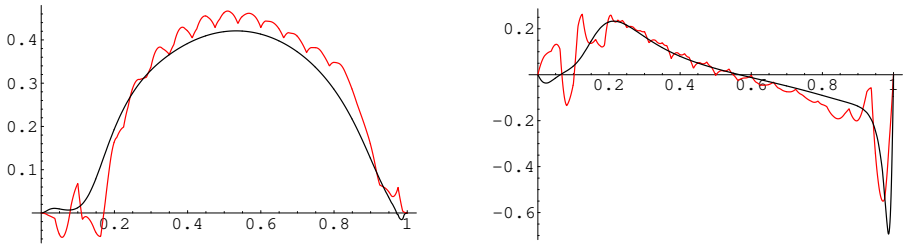

Fig. 6. u and v components of GSV-16 and GSV-64 discretizations on the straight line $y = 0.9$

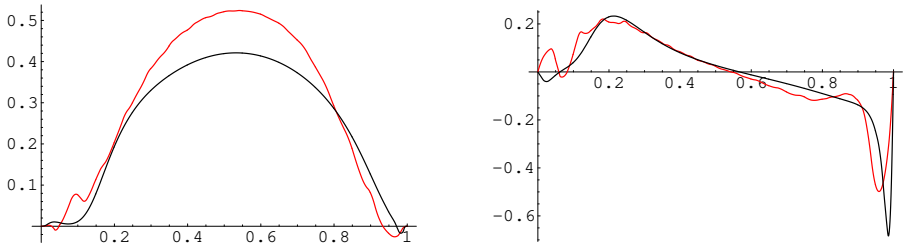

Fig. 7. u and v components of SSV-16 and SSV-64 discretizations on the straight line $y = 0.9$

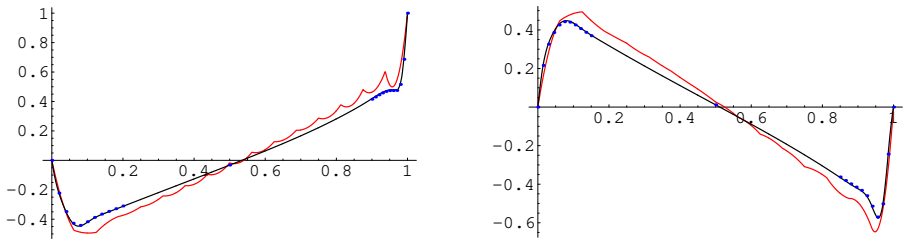

Fig. 8. u resp. v components of GSV-16 and GSV-64 discretizations on the straight line $x = 0.5$ resp. $y = 0.5$

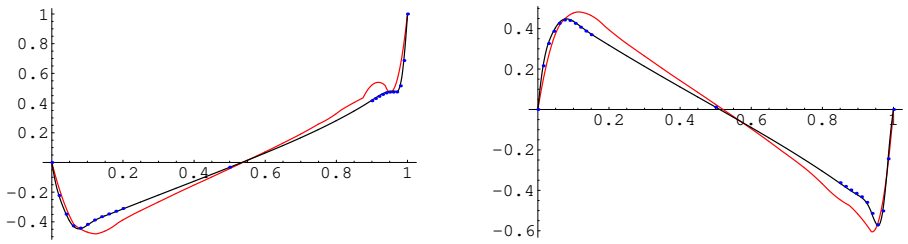

Fig. 9. u resp. v components of SSV-16 and SSV-64 discretizations on the straight line $x = 0.5$ resp. $y = 0.5$

Acknowledgements

First, we have to thank Klaus Gärtner from the Weierstrass Institute for Applied Analysis and Stochastics (WIAS) in Berlin for the many hours that he

spent discussing with the second author and for the direct solver PARDISO. Second, we have to thank Eberhard Bänsch having supported this research by valuable and constructive commentary and his advice to use the finite element toolbox ALBERTA. Third, we thank Manfred Uhle and Gerd Reinhardt from the WIAS in Berlin for their time-consuming assistence in producing the vector graphics in this publication. Last, but not least, we have to thank the DFG Research Center MATHEON in Berlin, which has funded the second author's research for 2 years and 10 months in the MATHEON project C2 *Efficient simulation of flows in semiconductor melts*. Further, MATHEON has financed a two day research stay of the first author in Berlin.

References

[1] D. N. Arnold and J. Qin. Quadratic velocity/linear pressure stokes elements. In R. Vichnevetsky, D. Knight, and G. Richter, editors, *Advances in Computer Methods for Partial Differential Equations VII*, pages 28–34. IMACS, 1992.

[2] R. Becker and M. Braack. A finite element pressure gradient stabilization for the stokes equations based on local projections. *Calcolo*, 38(4):173–199, 2001.

[3] M. Braack and E. Burman. Local projection stabilization for the oseen problem and its interpretation as a variational multiscale method. *SiNum*, 43(6):2544–2566, 2006.

[4] M. Braack, E. Burman, V. John, and G. Lube. Stabilized finite element methods for the generalized oseen problem. *submitted to Comput. Methods Appl. Mech. Engrg.*, 2005.

[5] E. Burman, M. Fernandez, and P. Hansbo. Edge stabilization for the incompressible navier-stokes equations: a continuous interior penalty finite element method. *to appear in SiNum*, 2004.

[6] E. Burman and M. A. Fernández. Stabilized finite element schemes for incompressible flow using velocity/pressure spaces satisfying the LBB-condition. In *Proceedings of the* 6^{th} *World Congress in Computational Mechanics, WCCM VI*, 2004.

[7] E. Burman and P. Hansbo. Edge stabilization for galerkin approximations of convection-diffusion-reaction problems. *Comput. Methods Appl. Mech. Engrg.*, 193:1437–1453, 2004.

[8] E. Burman and P. Hansbo. A stabilized non-conforming finite element method for incompressible flow. *Comput. Methods Appl. Mech. Engrg.*, 195(23-24):2881–2899, 2006.

[9] R. Codina. Stabilized finite element approximation of transient incompressible flows using orthogonal subscales. *Comput. Methods Appl. Mech. Engrg.*, 191(39-40):4295–4321, 2002.

[10] A. Ern and J. L. Guermond. *Theory and Practice of Finite Elements*, volume 159 of *Applied Mathematical Sciences*. Springer-Verlag, New York, 2004.

[11] E. Erturk, T. C. Corke, and C. Gökcöl. Numerical solutions of 2d-steady incompressible driven cavity flow at high reynolds numbers. *International Journal for Numerical Methods in Fluids*, 48:747–774, 2005.

[12] L. P. Franca and S. L. Frey. Stabilized finite element methods. ii. the incompressible navier-stokes equations. *Comput. Methods Appl. Mech. Engrg.*, 99(2–3):209–233, 1992.

[13] S. Ganesan and V. John. Pressure separation - a technique for improving the velocity error in finite element discretisations of the navier-stokes equations. *Applied Mathematics and Computation*, 165(2):275–290, 2005.

[14] K. Gärtner and O. Schenk. Solving unsymmetric sparse systems of linear equations with pardiso. In *Computational science —ICCS 2002, Part II*, Lecture Notes in Computational Science, pages 355–363, Berlin, 2002. ICCS.

[15] T. Gelhard, G. Lube, M. A. Olshanskii, and J.-H. Starcke. Stabilized finite element schemes with LBB-stable elements for incompressible flows. *J. Comput. Appl. Math.*, 177(2):243–267, 2005.

[16] U. Ghia, K. N. Ghia, and C. T. Shin. High-re solutions for incompressible flow using the navier-stokes equations and a multigrid method. *Journal of Computational Physics*, 48:387–411, 1982.

[17] P. Hansbo and A. Szepessy. A velocity-pressure streamline diffusion finite element method for the incompressible Navier-Stokes equations. *Comput. Methods Appl. Mech. Engrg.*, 84(2):175–192, 1990.

[18] V. John and S. Kaya. A finite element variational multiscale method for the Navier-Stokes equations. *SIAM J. Sci. Comput.*, 26(5):1485–1503 (electronic), 2005.

[19] C. Johnson and J. Saranen. Streamline diffusion methods for the incompressible Euler and Navier-Stokes equations. *Math. Comp.*, 47(175):1–18, 1986.

[20] U. Nävert. *A Finite Element Method for Convection-Diffusion Problems*. PhD thesis, Chalmers University of Technology, 1982.

[21] M. A. Olshanskii and A. Reusken. Grad-div stabilization for Stokes equations. *Math. Comp.*, 73(248):1699–1718 (electronic), 2004.

[22] O. Schenk, K. Gärtner, and W. Fichtner. Efficient sparse lu factorization with left-right looking strategy on shared memory multiprocessors. *BIT*, 40(1):158–176, 1999.

[23] A. Schmidt and K. G. Siebert. *Design of Adaptive Finite Element Software - The Finite Element Toolbox ALBERTA*, volume 42 of *Lecture Notes in Computational Science and Engineering*. Springer-Verlag, Berlin, 2005.

[24] L. Scott and S. Zhang. Finite element interpolation of nonsmooth functions satisfying boundary conditions. *Math. Comp.*, 54(190):483–493, 1990.

[25] L. R. Scott and M. Vogelius. Norm estimates for a maximal right inverse of the divergence operator in spaces of piecewise polynomials. *Mathematical Modelling and Numerical Analysis*, 19(1):111–143, 1985.

[26] L. Tobiska and R. Verfürth. Analysis of a streamline diffusion finite element method for the Stokes and Navier-Stokes equations. *SIAM J. Numer. Anal.*, 33(1):107–127, 1996.

[27] S. Zhang. A new family of stable mixed finite elements for the 3d stokes equations. *Math. Comp.*, 74(250):543–554, 2005.